NANO LETTERS
Letter
Cite This: Nano Lett. 2018, 18, 934–940
pubs.acs.org/NanoLett

Ultrafast Graphene Light Emitters

Young Duck Kim,[*,†,◐] Yuanda Gao,[‡,◐] Ren-Jye Shiue,[∥] Lei Wang,[⊥] Ozgur Burak Aslan,[#,▽] Myung-Ho Bae,[○,◆] Hyungsik Kim,[§] Dongjea Seo,[¶] Heon-Jin Choi,[¶] Suk Hyun Kim,[#,▽] Andrei Nemilentsau,[⊙] Tony Low,[⊙] Cheng Tan,[‡,§] Dmitri K. Efetov,[∥,●] Takashi Taniguchi,[⊕] Kenji Watanabe,[⊕] Kenneth L. Shepard,[§] Tony F. Heinz,[#,▽] Dirk Englund,[∥] and James Hone[*,‡]

[†]Department of Physics, Kyung Hee University, Seoul 02447, Republic of Korea
[‡]Department of Mechanical Engineering and [§]Department of Electrical Engineering, Columbia University, New York, New York 10027, United States
[∥]Department of Electrical Engineering and Computer Science, Massachusetts Institute of Technology, Cambridge, Massachusetts 02139, United States
[⊥]Kavli Institute at Cornell for Nanoscale Science, Ithaca, New York 14853, United States
[#]Department of Applied Physics, Stanford University, Stanford, California 94305, United States
[▽]SLAC National Accelerator Laboratory, Menlo Park, California 94025, United States
[○]Korea Research Institute of Standards and Science, Daejeon 34113, Republic of Korea
[◆]Department of Nano Science, University of Science and Technology, Daejeon 34113, Republic of Korea
[¶]Department of Materials Science and Engineering, Yonsei University, Seoul 120-749, Republic of Korea
[⊙]Department of Electrical and Computer Engineering, University of Minnesota, Minneapolis, Minnesota 55455, United States
[●]ICFO-Institut de Ciencies Fotoniques, The Barcelona Institute of Science and Technology, 08860 Castelldefels, Barcelona, Spain
[⊕]National Institute for Materials Science, 1-1 Namiki, Tsukuba 305-0044, Japan

Supporting Information

ABSTRACT: Ultrafast electrically driven nanoscale light sources are critical components in nanophotonics. Compound semiconductor-based light sources for the nanophotonic platforms have been extensively investigated over the past decades. However, monolithic ultrafast light sources with a small footprint remain a challenge. Here, we demonstrate electrically driven ultrafast graphene light emitters that achieve light pulse generation with up to 10 GHz bandwidth across a broad spectral range from the visible to the near-infrared. The fast response results from ultrafast charge-carrier dynamics in graphene and weak electron-acoustic phonon-mediated coupling between the electronic and lattice degrees of freedom. We also find that encapsulating graphene with hexagonal boron nitride (hBN) layers strongly modifies the emission spectrum by changing the local optical density of states, thus providing up to 460% enhancement compared to the gray-body thermal radiation for a broad peak centered at 720 nm. Furthermore, the hBN encapsulation layers permit stable and bright visible thermal radiation with electronic temperatures up to 2000 K under ambient conditions as well as efficient ultrafast electronic cooling via near-field coupling to hybrid polaritonic modes under electrical excitation. These high-speed graphene light emitters provide a promising path for on-chip light sources for optical communications and other optoelectronic applications.

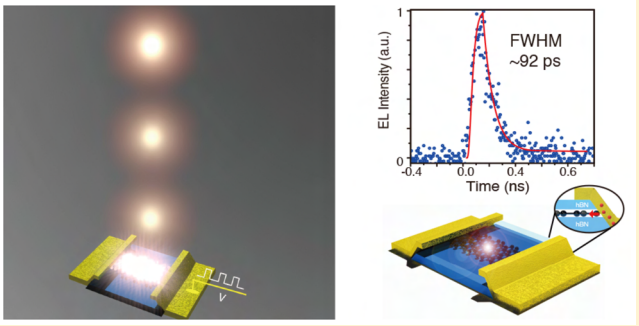

KEYWORDS: *Graphene, ultrafast light emitter, thermal radiation, van der Waals heterostructure, optoelectronics*

Intense research over the past decades has focused on the development of high-bandwidth photonics for inter- and intra-chip connections and other applications, with a specific aim at nanophotonic building blocks such as waveguides, optical modulators, and photodetectors. However, on-chip light sources, particularly monolithic nanoscale light sources with direct high-speed modulation, have remained challenging.[1] Due to its unique electronic and optical properties, graphene has emerged as a promising material for optoelectronic applications, including as ultrafast and broadband photodetectors,[2,3] optical modulators,[4,5] plasmonics,[6−8] and nonlinear photonic devices.[9] Previous graphene devices have shown the feasibility

Received: October 9, 2017
Revised: December 23, 2017
Published: January 16, 2018

Downloaded via UNIV OF CALIFORNIA SANTA BARBARA on February 15, 2019 at 08:33:53 (UTC).
See https://pubs.acs.org/sharingguidelines for options on how to legitimately share published articles.

© 2018 American Chemical Society

DOI: 10.1021/acs.nanolett.7b04324
Nano Lett. 2018, 18, 934–940

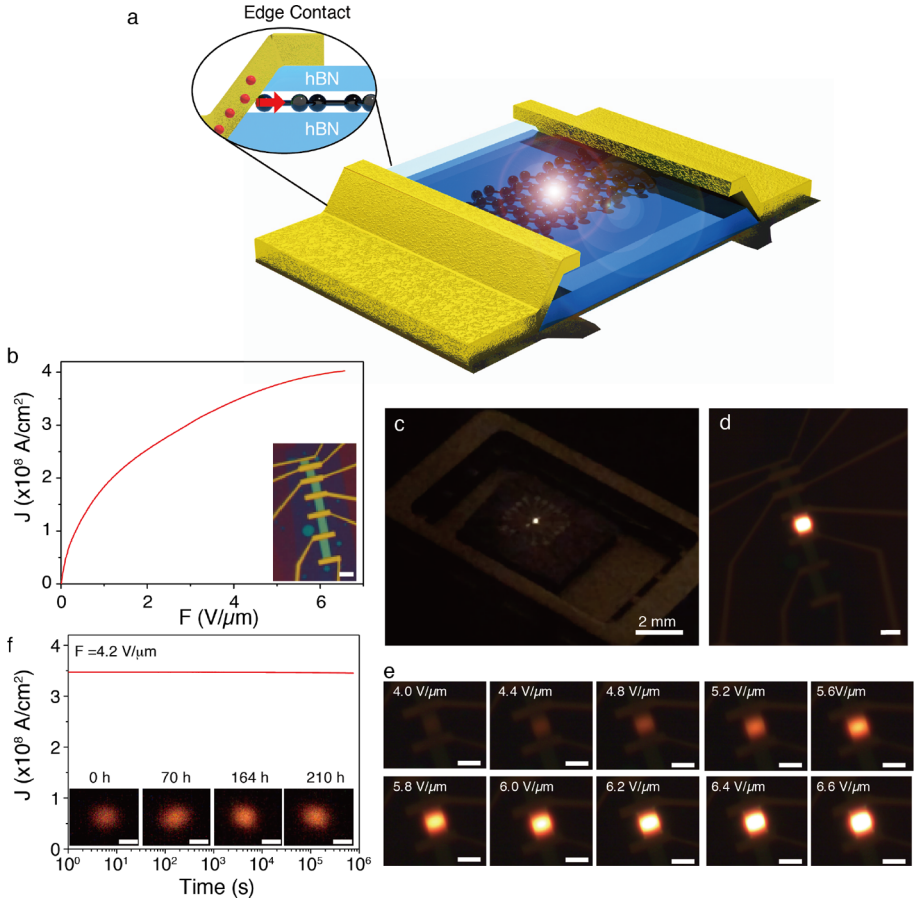

Figure 1. Ultrafast hBN encapsulated graphene thermal light emitter. (a) The device consists of a monolayer graphene encapsulated on top and bottom by hBN; it has a one-dimensional edge contact to the drain and source contact (see inset). (b) Current density (J) as a function of applied electric field (F) for an emitter with channel length of 5 μm and width of 3 μm (see inset with scale bar of 6 μm). (c) Optical images show bright visible light emission from a microscale (3−8 μm) individual graphene light emitter under applied electric field (F = 6 V/μm). (d,e) The graphene surface uniformly emits across the entire graphene/hBN heterostructures (3−6 μm) (d) and radiation intensity increase by the applied electric field (e). (Scale bar of 6 μm). (f) Long-term stability of graphene light emitter under vacuum. The current density (J) of graphene light emitter under constant electric field (F = 4.2 V/μm) was measured during 10^6 seconds (over 270 h), showing negligible variation in current density and light emission intensity. Inset shows the optical images. (Scale bar of 6 μm).

of ultrafast signal processing and frequency conversion functionalities required for photonic integrated circuits.[9,10]

Graphene's high thermal stability, low heat capacity, and ultrafast optoelectronic properties[3,11] suggest that it could function as an unusual fast and efficient thermal light emitter. Early efforts showed infrared light emission from SiO_2-supported graphene, with temperatures limited to ∼1100 K[12−14] due to dielectric degradation at high temperature[15] and significant hot carrier cooling to the substrate. We recently demonstrated thermal light emission in the visible range from electrically biased suspended graphene,[16] which achieves temperature up to ∼2800 K. However, to achieve rapid cooling required for fast modulation and to integrate such devices into photonic platforms, a substrate-supported device design is needed. Moreover, little is known about the possible modulation rate of graphene thermal emitters under electrical excitation.

Here, we demonstrate electrically driven ultrafast thermal light emitters based on hBN-encapsulated graphene. The hBN allows roughly 60% larger current density than for SiO_2-supported graphene due to its larger optical phonon energy[17] and, at the same time, provides excellent encapsulation. As a result, our devices achieve electron temperatures up to 2000 K and produce broadband emission extending up to the visible range. Our studies further indicate device lifetimes of years in vacuum and good stability even under ambient conditions. The thermal emission spectrum is strongly modified by the hBN dielectric optical cavity,[5,18] which provides 460% enhancement for a broad peak centered at 720 nm compared to the gray-body thermal radiation. Analysis of thermal transport in the devices shows that the hBN effectively spreads heat over the micron scale, and that the dominant thermal transport pathway is vertical, with good agreement between models and the measured power consumption and temperature profile. Independent measurements of electron and acoustic phonon temperatures indicate that the electrons can be ∼30% hotter than the acoustic phonons at high bias due to weak electron-acoustic phonon coupling.[11,19] Studies of the light emission under radiofrequency and pulsed electrical excitation show continuous modulation at 3 GHz and emission pulses of 92 ps full width at half-maximum (fwhm). Our demonstration of ultrafast light pulse generation by electrical excitation is consistent with a model in which electrons are strongly coupled to hybrid plasmon−phonon polariton modes at the graphene−hBN interface but out of equilibrium with the acoustic phonons.

DOI: 10.1021/acs.nanolett.7b04324
Nano Lett. 2018, 18, 934−940

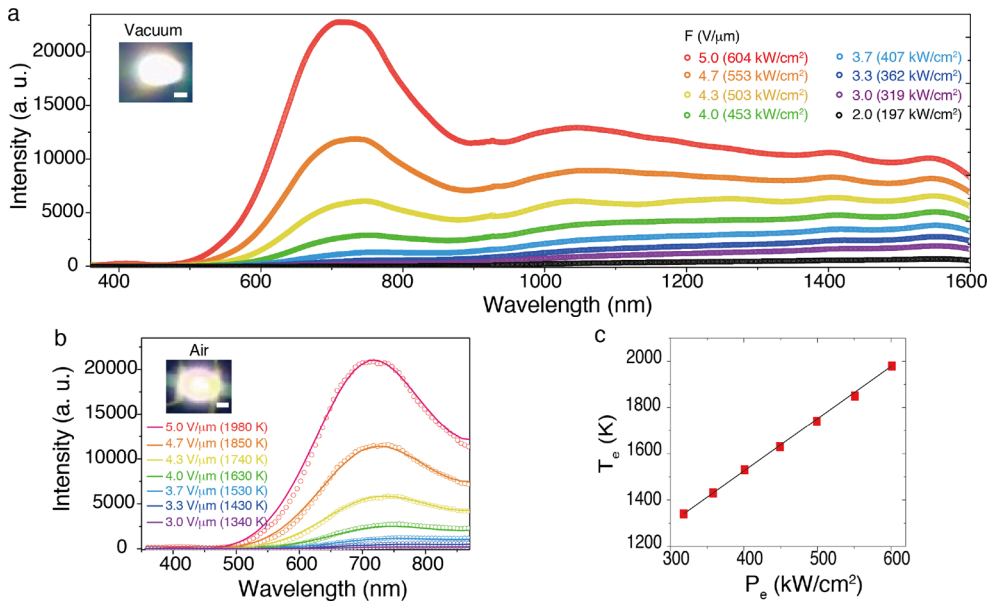

Figure 2. Radiation spectrum of graphene light emitter under vacuum and air. (a) Measured radiation spectrum of graphene light emitter (scatter) under vacuum with various F and electric power. We find an emission peak at the around 718 nm and a flat response at the near-infrared range for high F values. Inset shows the optical image of visible light emission under F = 5.0 V/μm. (Scale bar is 6 μm). (b) Measured radiation spectrum of graphene light emitter (scatter) under air and calculated thermal radiation (solid line) based on the estimated electron temperature and gray-body thermal radiation by Planck's law with strong light-matter interaction. Inset shows the optical image of visible light emission under F = 4.3 V/μm. (Scale bar is 6 μm). (c) T_e as a function of P_e under air (red square). Solid line is a linear fit to the data.

To fabricate the graphene light emitters, hBN/graphene/hBN heterostructures were first assembled by a van der Waals dry pick-up method using exfoliated monolayer graphene and exfoliated hBN flakes with 10−20 nm thickness and transferred to a SiO_2 (285 nm)/Si substrate, as shown in Figure 1a. Electrical contacts were formed by etching the assembled heterostructure and depositing metal (Cr/Pd/Au) on the exposed edge.[20] The resulting graphene heterostructure exhibits mobility near the intrinsic acoustic phonon scattering limit at room temperature.[20] The atomically clean interface reduces extrinsic effects[21,22] such as surface roughness, defects and charged impurities. This permits the investigation of intrinsic electro-thermal properties, including thermal radiation, energy dissipation, and ultrafast dynamics of hot electrons in the disorder-free graphene system.

Under high electric fields (F) up to ~6.6 V/μm and zero back gate voltage (V_{BG}), these devices achieve current density (J) up to ~4.0 × 10^8 A/cm^2 as shown in Figure 1b. This high current density is due both to the high stability of the hBN and its high optical phonon energy, as will be explored further below. At high current density, we observe remarkably bright visible light emission from these micron-scale structures, even observable by the naked eye, as shown in Figure 1c. The emission is seen across the channel region and increases in intensity with F as shown in Figure 1d,e (see the movies in the Supporting Information).

Because stability is essential for practical applications, we tested the long-term performance of the graphene light emitter under high electric field (F = 4.2 V/μm) and high current density (J ≈ 3.4 × 10^8 A/cm^2) under ~10^{-5} Torr vacuum. These measurements showed no significant degradation of emission intensity and electrical current over a test period of ~10^6 seconds as shown in Figure 1f, suggesting a device lifetime (defined by 50% degradation in current) exceeding 4 years. This result attests to the remarkable stability of both the hBN encapsulation[23,24] and edge contacts even under high electric field, current density, and temperature. Important for practical applications, we also observed visible light emission under ambient conditions: the best devices showed stable operation in air for several days, and it is likely that improved encapsulation will extend this lifetime.

Figure 2a shows the spectrum of the emitted light for a range of applied electric fields (or electric powers) under vacuum conditions. The spectrum extends from the visible to near-infrared (400−1600 nm), with an emission peak around 720 nm and a flat response in the near-infrared (>1000 nm) from several graphene light emitters. The spectrum is unchanged for emission in air (Figure 2b). The strong emission peak at 720 nm from the hBN encapsulated graphene light emitter can be attributed to the formation of a dielectric optical cavity by the hBN layers (refractive index n = 2.2) on SiO_2/Si substrate and the resulting in tailoring of thermal radiation by the modified local optical density of states.[25] Based on the tailored of thermal radiation of graphene light emitter, we estimate the maximum T_e = 1980 K for F = 5.0 V/μm (solid lines in Figure 2b for various values of F). We also found that the radiation enhancement reaches 460% at the 720 nm peak relative to graphene gray-body thermal radiation at same T_e,[25] as detailed in the Supporting Information. We note that the observed flat spectral response in the near-infrared (>1000 nm) regime can be attributed to the Pauli blocking by thermal excited electrons, which reduces the graphene absorptivity (emissivity).

Figure 2c shows that the derived T_e increases roughly linearly with applied electrical power density (P_e), indicating that the dominant heat-transfer mechanism is by vertical conduction through the substrate rather than radiation. Consistent with this observation, dividing the total output optical power (P_r) across all wavelengths based on the Stefan−Boltzmann law by P_e, we find a radiation efficiency of η ≈ 3.45 × 10^{-6} (see the Supporting Information). This is smaller than obtained for

DOI: 10.1021/acs.nanolett.7b04324
Nano Lett. 2018, 18, 934−940

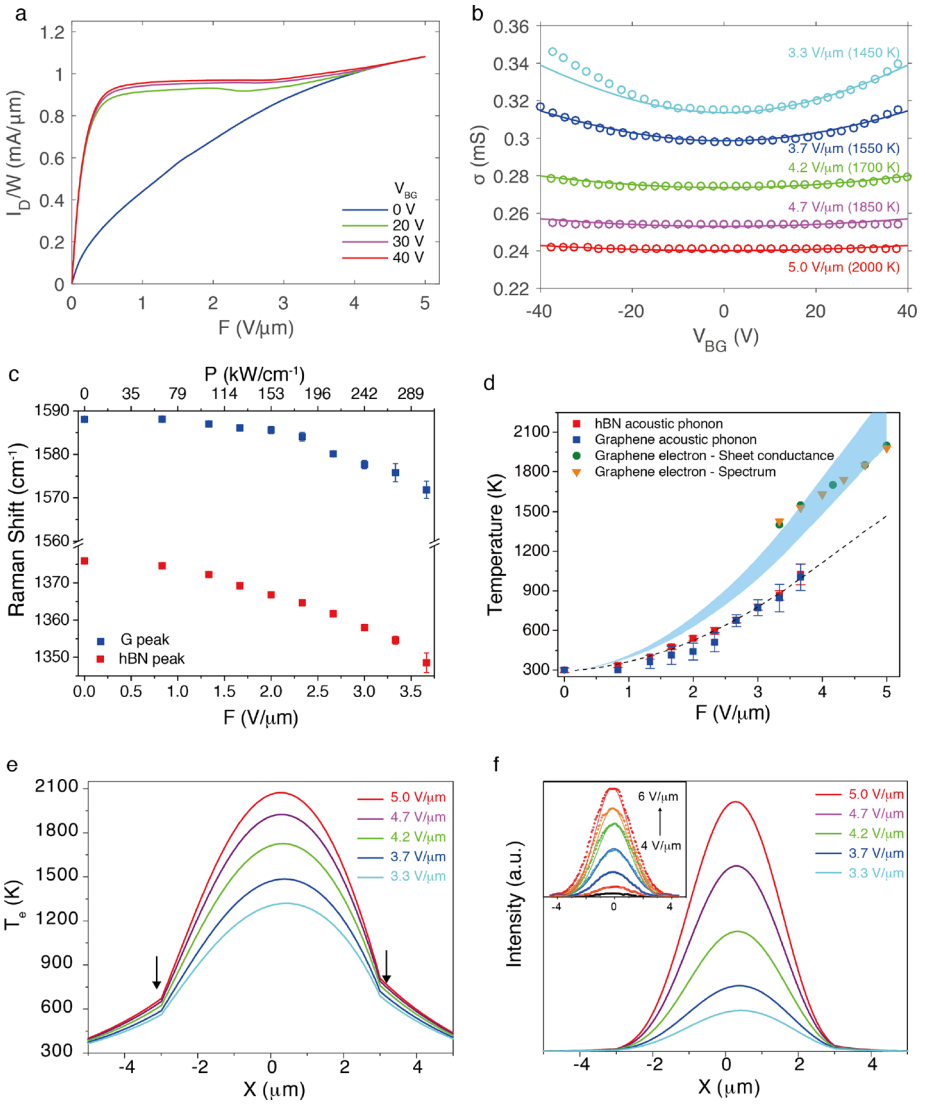

Figure 3. Electronic and lattice temperatures in the graphene light emitter. (a) Current as a function of applied electric field (F) for various gate voltage (V_{BG}). Above the critical electric field ($F > 4$ V/μm), current levels are not changed by V_{BG}. (b) Sheet conductance (σ) modulation by V_{BG} of graphene heterostructure for various F. The electron temperature (T_e) is estimated based on a simulation of thermally generated charge carriers by F. Experimental data (scatter) and simulation (solid line) of σ agree well. (c) Raman spectroscopy of graphene/hBN heterostructure to estimate the lattice temperature (T_{ap}). Raman peak shift of the hBN E_{2g} and graphene G modes as a function of F. (d) Decoupling of electron and lattice temperature in graphene light emitters. Values of T_e are calculated from the emission spectrum (orange triangles) and σ modulation (green circles), and the T_{ap} of graphene (blue squares) and hBN (red squares) are estimated from the Raman peak shift. The black dashed line is fitting of T_{ap} and the shaded region is obtained for nonequilibrium temperature coefficients $\alpha \sim 0.45$–0.77. (e, f) Calculated T_e profile of the graphene light emitter for various values of F (arrows indicate the edge of metal electrodes). (f) Calculated radiation intensity profile for various values of F based on the temperature profile and the Stefan–Boltzmann law. (Inset, measured optical intensity profile (scatter) and Gaussian fitting (solid line) based on the optical images of Figure 1e.).

suspended graphene but can be improved by optical and thermal engineering.

To provide a second measurement of T_e, we analyzed the high-bias electrical transport behavior. We observed that the I–V behavior of hBN encapsulated graphene for different values of the V_{BG} (Figure 3a) showed current saturation[16,17,26] under modest electrical fields ($F > 0.5$ V/μm) for $V_{BG} > 20$ V. This saturation can be attributed to efficient backscattering of electrons by emission of optical phonons in either the graphene or the hBN substrate. The optical phonon activation length $L_\Omega (\propto \hbar\Omega/F$, where $\hbar\Omega$ is the optical phonon energy of 150–200 meV)[27,28] becomes comparable to the acoustic phonon scattering length (~1 μm in a hBN encapsulated graphene at room temperature[20]) at $F > 0.3$–0.4 V/μm, consistent with the observed onset of current saturation. The observed saturation is also consistent with optical studies that show highly efficient scattering of hot electrons to optical phonons. In SiO_2-supported devices, visible light emission is different because hot electrons can emit SiO_2 optical phonons with lower energy ($\hbar\Omega_{SiO_2} \approx 60$–$80$ meV), resulting in a lower current density (Figure S4). Finally, we note the presence of a "kink" in the I–V curves above 2 V/μm. The origin of this kink is unclear, but similar structures seen in metallic carbon nanotube devices have been attributed to the evaporation of adsorbates, abrupt change in the nonequilibrium phonon population, and finite doping due to defect creations.[28]

DOI: 10.1021/acs.nanolett.7b04324
Nano Lett. 2018, 18, 934–940

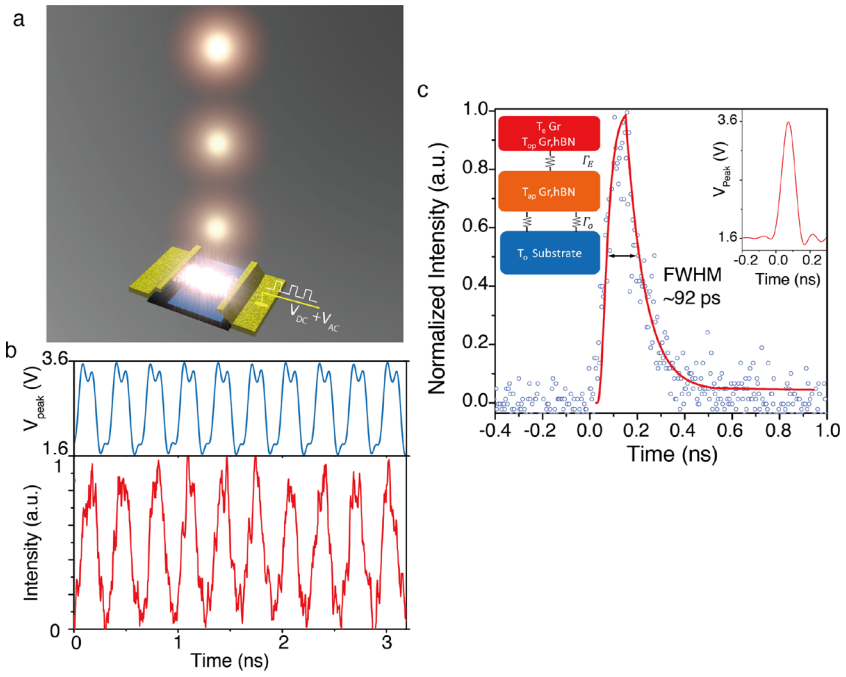

Figure 4. Generation of ultrafast light pulses by the electric control. (a) Schematic of the electrically driven ultrafast graphene light emitter. The temporal profile of the light pulses are recorded by time-correlated single-photon counting. (b) Emission profiles (lower panel) for pulsed electrical excitation (upper panel). The emission profile follows the electrical drive at the indicated frequency of ~3 GHz. (c) Generation of ultrafast (92 ps) light pulses from the graphene light emitter (blue solid line) for an 80 ps electrical drive pulse, corresponding to a bandwidth of 10 GHz. According to the transit temperature and thermal radiation exponential fit (red solid lines). Left inset: schematic of energy relaxation of graphene. The red block corresponds to quasi-equilibrium of electrons of in graphene and the strongly coupled optical phonons of the graphene/hBN by hybrid polaritonic modes under electrical excitation. Subsequently, the heat flows to the acoustic phonons and the substrate. Right inset: temporal profile of the 80 ps electrical drive pulse.

We also measured T_e by plotting sheet conductance (σ) against V_{BG} for different values of F (Figure 3b). For $F < 3.3$ V/μm, σ is clearly modulated by V_{BG}, while above 4 V/μm, σ is nearly independent of V_{BG}. This reduction in gate modulation occurs when the density of thermally generated charge carriers exceeds the electrostatically induced charge carrier density, providing a measure of the electronic temperature. Numerical calculations of the graphene self-heating show good agreement with the measured (Figure 3b, solid lines) (see the Supporting Information for details). The derived values of T_e are close to those obtained from fitting the radiation spectrum (Figure 2b).

We next measured the acoustic phonon temperature T_{ap} of graphene and hBN by Raman spectroscopy: the graphene G mode and the hBN E_{2g} modes shift downward with increasing T_{ap} due to anharmonic phonon coupling[29] (see the Supporting Information for detail). Figure 3c shows the variation of these modes up to $F = 3.7$ V/μm, above which the visible radiation background interfered with the measurement. Figure 3d shows the derived temperatures, together with the electronic temperature derived above. At high bias, the T_{ap} of the graphene and hBN are nearly equal but below the electronic temperature. The measured values are well fit by $T_e = T_{ap} + \alpha(T_{ap} - T_0)$, where T_0 is the ambient temperature, with $\alpha \approx 0.45-0.77$.[16,30,31] Based on the measured T_e and T_{ap} in the hBN encapsulated graphene heterostructure under electrical excitation, we find $\alpha \approx 0.45-0.77$. However, given the uncertainty in calibration of the Raman shift rates with temperature and possible confounding effects such as substrate thermal expansion, this result alone is not sufficient to definitively establish the disequilibrium between T_e and T_{ap}. Because heat dissipation occurs primarily through transport of acoustic phonons, we used the measured T_{ap} to calculate the total vertical thermal resistance to the ambient, $R_{th} \approx 10\,650-11\,480$ K/W. This value matches reasonably well with a simple model in which heat flow is dominated by vertical transport through the hBN and SiO_2 to the Si substrate and is dominated by the thermal resistance of SiO_2 layer[32] (see the Supporting Information and Table S1).

Combining the vertical thermal transport results above with the lateral thermal conductivity of the hBN allows the calculation of the lateral thermal diffusion (healing) length $L_H \approx 1.3$ μm. Combining this value with the nonequilibrium electronic temperature allows the calculation of the spatial variation of T_e (see the Supporting Information). Figure 3e plots the resulting T_e distribution along the graphene light emitter for various values of F based on the heat diffusion equation of T_{ap} and nonequilibrium temperature coefficient α (see the Supporting Information). In all cases, the cooling to the substrate keeps T_e near the metal electrodes below ~600 K, explaining the high stability of the devices. The expected thermal radiation intensity profile based on the modeled temperature distribution is shown in Figure 3f, in good agreement with the measured optical intensity profile (see Figure 3f inset and the Supporting Information).

The small size and low heat capacity of the graphene emitter presents an opportunity for ultrafast thermal emission modulation. Moreover, measurement of the dynamics of light modulation under electrical pulses may provide insight into the carrier dynamics and offer another means to examine whether electron and phonon populations are out of equilibrium under high electric field. Moreover, recent theoretical and ultrafast photocurrent[33,34] studies also suggest that direct electronic

DOI: 10.1021/acs.nanolett.7b04324
Nano Lett. 2018, 18, 934−940

cooling into hBN can be mediated by efficient near-field heat transfer due to the hybrid plasmon−phonon polaritonic mode at the highly localized graphene−hBN interface[34] by optical excitation. Therefore, we examined the ultrafast response of a device fabricated on a quartz substrate under electrical excitation, which reduces parasitic capacitance and enables electrical driving at GHz frequencies with DC offset bias (V_{DC}) (Figure 4); the device exhibits identical steady-state radiation as observed above for the SiO_2/Si substrate-mounted devices. As a first test, the emission time trace in Figure 4b shows on−off modulation with near-perfect contrast when device is driven with a continuous 3 GHz signal. For an even shorter pulse duration (fwhm 80 ps, peak to peak 2 V with V_{DC} = 1.6 V), the output light pulse width is only broadened to 92 ps (fwhm), which corresponding to above 10 GHz bandwidth as shown in Figure 4c. This response is many orders of magnitude faster than conventional thermal radiation sources based on bulk materials, for which modulation speed has been limited to ∼100 Hz.[35]

This observed ultrafast response may arise from the small size and thermal mass of the graphene because vertical thermal diffusion can occur over sub-nanosecond time scales for nanometer-scale structures. More intriguingly, if electrons are out of equilibrium with the acoustic phonons as indicated in Figure 3d, this high speed may be due to ultrafast cooling from T_e to T_{ap}, which should be sufficient to modulate the output intensity by direct electronic cooling mediated with near-field heat transfer via hybrid plasmon−phonon polaritonic mode at graphene−hBN interfaces.

To understand the dynamics, we consider a simple heat-transfer model (Figure 4C, inset) in which the hot graphene electrons are strongly coupled to and in equilibrium with the optical phonons of graphene and the top few layers of the hBN.[19,34] These optical phonons are connected to the acoustic phonon bath by thermal conductance Γ_E and then to the environment by Γ_0.[36] The observed difference in the electronic and acoustic phonon temperatures, $T_e - T_{ap} \approx P/\Gamma_E$,[36] provides a measure of $\Gamma_E \approx 6.0-8.4$ MW m^{-2} K^{-1}, which is consistent with theory.[37] The measured time constant for cooling τ_c then provides a measure of the heat capacity of the electron/optical phonon system, $C_T = \tau_c\Gamma_E = 0.72-6.63 \times 10^{-3}$ J m^{-2} K^{-1}. This value is considerably larger than the electronic heat capacity alone (see the Supporting Information), supporting the assumption that optical phonons are in equilibrium with the electrons. We find that the magnitude of C_T corresponds to that of optical phonons in graphene in addition to 0.3−3.6 nm of the surrounding hBN.[38,39] This view is consistent with theoretical predictions for hybrid modes that are highly localized at the graphene-hBN interface.[33,34]

This work establishes that hBN-encapsulated graphene provides visible light emission with high stability and a modulation rate speed several orders of magnitude faster than conventional thermal emitters. This exceptional speed likely arises because hot electrons are strongly coupled to optical phonons and hybrid plasmon−hyperbolic phonon polariton modes in hBN under electrical excitation but weakly coupled to acoustic phonons. Future devices making use of a tunable energy relaxation pathway for the graphene light emitter, such as tunneling structures,[40] could allow light modulation beyond the speed limits explored here. This high speed may render these graphene emitters suitable for use in optical communications. A necessary next step toward this goal would be to demonstrate narrowband emission with enhanced efficiency. The observed strong modification of the emission by the optical modes in the hBN slab provides proof of principle that the thermal emission can be tailored by engineering of the optical cavity, and previous work has already demonstrated that integrating graphene with resonant optical structures crystal cavities can be used for narrow-band absorption. Alternatively, broadband and high-speed light sources are of interest for other applications such as on-chip spectroscopy. Finally, we note that graphene thermal emitters employ the same basic device architecture as demonstrated previously for ultrafast photodetectors and electro-optic modulators.[2,5,8] Thus, one graphene−hBN heterostructure device could serve three essential electro-optic device functions, which could enable flexible and reconfigurable electro-optic applications in future photonic system architectures.

■ ASSOCIATED CONTENT

Supporting Information

Supporting Information is available free of charge at The Supporting Information is available free of charge on the ACS Publications website at DOI: 10.1021/acs.nanolett.7b04324.

Figures showing low electric field transport at room temperature, graphene light emitters, a comparison of radiation spectra, numerican calculation of current density, numerical calculation of graphene on substrates, charge-carrier concentration, energy dissipation, optical image intensity profiles, Raman peak shifts, current saturation and negative differential conductance, transient temperatures, time-resolved light-emission intensity, estimated cooling time constants, calculated specific heat, and calculated transient electron and phonon temperature. Additional details on the tailoring of thermal radiation intensity of graphene light emitter with hBN layers, TM waves, electro-thermal calculation of graphene light emitter under high electric fields, Raman spectroscopy, optical spectroscopy, time-resolved light emission, electrical RC time constants, current saturation and negative differential conductance, and thermal radiation efficiency. Tables showing thermal conductance and transient heating and cooling rates (PDF)

Movie clip of bright visible light emission from a microscale (3−6 μm) individual graphene light emitter under applied electric field sweep up (0 ∼ 6.6 V/μm) and sweep down (6.6 − 0 V/μm), captured under microscope (Figure 3d, e are part of this movie clip) (AVI)

Movie clip of bright visible light emission from a microscale (3−8 μm) individual graphene light emitter under applied electric field sweep up (0 ∼ 6 V/μm) and sweep down (6−0 V/μm), captured from out of vacuum chamber (Figure 3c is part of this movie clip) (AVI)

■ AUTHOR INFORMATION

Corresponding Authors

*E-mail: ydk@khu.ac.kr.
*E-mail: jh2228@columbia.edu.

ORCID

Young Duck Kim: 0000-0003-2593-9826
Lei Wang: 0000-0002-1919-9107
Ozgur Burak Aslan: 0000-0002-0925-3026
Hyungsik Kim: 0000-0003-1921-4175

DOI: 10.1021/acs.nanolett.7b04324
Nano Lett. 2018, 18, 934−940

Andrei Nemilentsau: 0000-0002-0895-5181
Tony Low: 0000-0002-5759-5899
Dmitri K. Efetov: 0000-0001-5862-0462
Kenji Watanabe: 0000-0003-3701-8119
Tony F. Heinz: 0000-0003-1365-9464
Dirk Englund: 0000-0002-1043-3489

Author Contributions

◐Y.D.K. and Y.G. contributed equally.

Notes

The authors declare no competing financial interest.

■ ACKNOWLEDGMENTS

Y.D.K was partially supported by the Columbia University SEAS Translational Fellow program. At Columbia, device fabrication and electrical testing were supported by the Office of Naval Research, grant no. N00014-13-1-0662; optical spectroscopy was supported by DOE-BES grant no. DE-FG02-00ER45799. Ultrafast measurements at MIT were supported in part by the Center for Excitonics, an Energy Frontier Research Center funded by the U.S. Department of Energy, Office of Basic Energy Sciences under award no. DE-SC0001088. M.H.B was supported grants from the National Research Foundation of Korea (grant nos. NRF-2015R1A2A1A10056103 and SRC2016R1A5A1008184) funded by the Korea government. D.S. and H.C. were supported by NRF grant funded by the Korea government (no. 2017R1A2B3011586) and the third Stage of Brain Korea 21 Plus Project. A.N. and T.L were supported by a DARPA grant award no. FA8650-16-2-7640. K.W. and T.T acknowledge support from the Elemental Strategy Initiative conducted by the MEXT, Japan, and JSPS KAKENHI, grant no. JP15K21722. The Stanford authors acknowledge support by the National Science Foundation (grant no. DMR-1411107 for Raman measurements) and by the Air Force Office of Scientific Research (grant no. FA9550-12-1-0119 for emission measurements).

■ REFERENCES

(1) Zhou, Z.; Yin, B.; Michel, J. *Light: Sci. Appl.* **2015**, *4*, e358.
(2) Gan, X.; Shiue, R.-J.; Gao, Y.; Meric, I.; Heinz, T. F.; Shepard, K.; Hone, J.; Assefa, S.; Englund, D. *Nat. Photonics* **2013**, *7*, 883−887.
(3) J, T.; PiatkowskiL; MassicotteM; WoessnerA; MaQ; LeeY; S, M.; N, L.; Jarillo-HerreroP; van HulstN F; L, K. H. *Nat. Nano* **2015**, *10*, 437−443.
(4) Phare, C. T.; Daniel Lee, Y.-H.; Cardenas, J.; Lipson, M. *Nat. Photonics* **2015**, *9*, 511−514.
(5) Gao, Y.; Shiue, R.-J.; Gan, X.; Li, L.; Peng, C.; Meric, I.; Wang, L.; Szep, A.; Walker, D.; Hone, J.; Englund, D. *Nano Lett.* **2015**, *15*, 2001−2005.
(6) Low, T.; Avouris, P. *ACS Nano* **2014**, *8*, 1086−1101.
(7) Grigorenko, A. N.; Polini, M.; Novoselov, K. S. *Nat. Photonics* **2012**, *6*, 749−758.
(8) Woessner, A.; Gao, Y.; Torre, I.; Lundeberg, M. B.; Tan, C.; Watanabe, K.; Taniguchi, T.; Hillenbrand, R.; Hone, J.; Polini, M.; Koppens, F. H. L. *Nat. Photonics* **2017**, *11*, 421−424.
(9) Bonaccorso, F.; Sun, Z.; Hasan, T.; Ferrari, A. C. *Nat. Photonics* **2010**, *4*, 611−622.
(10) Bao, Q.; Loh, K. P. *ACS Nano* **2012**, *6*, 3677−3694.
(11) Lui, C. H.; Mak, K. F.; Shan, J.; Heinz, T. F. *Phys. Rev. Lett.* **2010**, *105*, 127404.
(12) Freitag, M.; Chiu, H.-Y.; Steiner, M.; Perebeinos, V.; Avouris, P. *Nat. Nanotechnol.* **2010**, *5*, 497−501.
(13) Engel, M.; Steiner, M.; Lombardo, A.; Ferrari, A. C.; Löhneysen, H. V.; Avouris, P.; Krupke, R. *Nat. Commun.* **2012**, *3*, 906.
(14) Bae, M.-H.; Ong, Z.-Y.; Estrada, D.; Pop, E. *Nano Lett.* **2010**, *10*, 4787−4793.
(15) DiMaria, D. J.; Cartier, E.; Arnold, D. *J. Appl. Phys.* **1993**, *73*, 3367−3384.
(16) Kim, Y. D.; Kim, H.; Cho, Y.; Ryoo, J. H.; Park, C.-H.; Kim, P.; Kim, Y. S.; Lee, S.; Li, Y.; Park, S.-N.; Shim Yoo, Y.; Yoon, D.; Dorgan, V. E.; Pop, E.; Heinz, T. F.; Hone, J.; Chun, S.-H.; Cheong, H.; Lee, S. W.; Bae, M.-H.; Park, Y. D. *Nat. Nanotechnol.* **2015**, *10*, 676−681.
(17) Meric, I.; Han, M. Y.; Young, A. F.; Ozyilmaz, B.; Kim, P.; Shepard, K. L. *Nat. Nanotechnol.* **2008**, *3*, 654−659.
(18) Gan, X.; Mak, K. F.; Gao, Y.; You, Y.; Hatami, F.; Hone, J.; Heinz, T. F.; Englund, D. *Nano Lett.* **2012**, *12*, 5626−5631.
(19) Berciaud, S.; Han, M. Y.; Mak, K. F.; Brus, L. E.; Kim, P.; Heinz, T. F. *Phys. Rev. Lett.* **2010**, *104*, 227401.
(20) Wang, L.; Meric, I.; Huang, P. Y.; Gao, Q.; Gao, Y.; Tran, H.; Taniguchi, T.; Watanabe, K.; Campos, L. M.; Muller, D. A.; Guo, J.; Kim, P.; Hone, J.; Shepard, K. L.; Dean, C. R. *Science* **2013**, *342*, 614−617.
(21) Kim, Y. D.; Bae, M.-H.; Seo, J.-T.; Kim, Y. S.; Kim, H.; Lee, J. H.; Ahn, J. R.; Lee, S. W.; Chun, S.-H.; Park, Y. D. *ACS Nano* **2013**, *7*, 5850−5857.
(22) Cui, X.; Lee, G.-H.; Kim, Y. D.; Arefe, G.; Huang, P. Y.; Lee, C.-H.; Chenet, D. A.; Zhang, X.; Wang, L.; Ye, F.; Pizzocchero, F.; Jessen, B. S.; Watanabe, K.; Taniguchi, T.; Muller, D. A.; Low, T.; Kim, P.; Hone, J. *Nat. Nanotechnol.* **2015**, *10*, 534−540.
(23) Wang, L.; Chen, Z.; Dean, C. R.; Taniguchi, T.; Watanabe, K.; Brus, L. E.; Hone, J. *ACS Nano* **2012**, *6*, 9314−9319.
(24) Lee, G.-H.; Cui, X.; Kim, Y. D.; Arefe, G.; Zhang, X.; Lee, C.-H.; Ye, F.; Watanabe, K.; Taniguchi, T.; Kim, P.; Hone, J. *ACS Nano* **2015**, *9*, 7019−7026.
(25) Ilic, O.; Bermel, P.; Chen, G.; Joannopoulos, J. D.; Celanovic, I.; Soljačić, M. *Nat. Nanotechnol.* **2016**, *11*, 320−324.
(26) Serov, A. Y.; Ong, Z.-Y.; Fischetti, M. V.; Pop, E. *J. Appl. Phys.* **2014**, *116*, 034507.
(27) Barreiro, A.; Lazzeri, M.; Moser, J.; Mauri, F.; Bachtold, A. *Phys. Rev. Lett.* **2009**, *103*, 076601.
(28) Amer, M.; Bushmaker, A.; Cronin, S. *Nano Res.* **2012**, *5*, 172−180.
(29) Bonini, N.; Lazzeri, M.; Marzari, N.; Mauri, F. *Phys. Rev. Lett.* **2007**, *99*, 176802.
(30) Kim, Y. D.; Bae, M. H. In *Advances in Carbon Nanostructures*; InTech: London, U.K., 2016; pp 83−100.
(31) Dorgan, V. E.; Behnam, A.; Conley, H. J.; Bolotin, K. I.; Pop, E. *Nano Lett.* **2013**, *13*, 4581−4586.
(32) Liu, Y.; Ong, Z.-Y.; Wu, J.; Zhao, Y.; Watanabe, K.; Taniguchi, T.; Chi, D.; Zhang, G.; Thong, J. T. L.; Qiu, C.-W.; Hippalgaonkar, K. *Sci. Rep.* **2017**, *7*, 43886.
(33) Kumar, A.; Low, T.; Fung, K. H.; Avouris, P.; Fang, N. X. *Nano Lett.* **2015**, *15*, 3172−3180.
(34) Principi, A.; Lundeberg, M. B.; Hesp, N. C. H.; Tielrooij, K.-J.; Koppens, F. H. L.; Polini, M. *Phys. Rev. Lett.* **2017**, *118*, 126804.
(35) Ali, S. Z.; De Luca, A.; Hopper, R.; Boual, S.; Gardner, J.; Udrea, F. *IEEE Sens. J.* **2015**, *15*, 6775−6782.
(36) Massicotte, M.; Schmidt, P.; Vialla, F.; Watanabe, K.; Taniguchi, T.; Tielrooij, K. J.; Koppens, F. H. L. *Nat. Commun.* **2016**, *7*, 12174.
(37) Low, T.; Perebeinos, V.; Kim, R.; Freitag, M.; Avouris, P. *Phys. Rev. B: Condens. Matter Mater. Phys.* **2012**, *86*, 045413.
(38) Cocemasov, A. I.; Nika, D. L.; Balandin, A. A. *Nanoscale* **2015**, *7*, 12851−12859.
(39) Vassiliev, V. P.; Gong, W.; Taldrik, A. F.; Kulinich, S. A. *J. Alloys Compd.* **2013**, *552*, 248−254.
(40) Ma, Q.; Andersen, T. I.; Nair, N. L.; Gabor, N. M.; Massicotte, M.; Lui, C. H.; Young, A. F.; Fang, W.; Watanabe, K.; Taniguchi, T.; Kong, J.; Gedik, N.; Koppens, F. H. L.; Jarillo-Herrero, P. *Nat. Phys.* **2016**, *12*, 455−459.

DOI: 10.1021/acs.nanolett.7b04324
Nano Lett. 2018, 18, 934−940